Tomographic PIV Assessment of Turbulence Characteristics in the Developing Region of a Turbulent Round Jet

Morteza Khashehchi[1,*], Gerrit E. Elsinga[3], Kamel Hooman[1], Andrew Ooi[2], Julio Soria[4], Ivan Marusic[2]

1: School of Mechanical and Mining Engineering, University of Queensland, QLD 4072, AUSTRALIA.

2: Department of Mechanical Engineering, University of Melbourne, Victoria, 3010, AUSTRALIA.

3: Department of Aerospace Engineering, TU-Delft, The Netherlands.

4: Laboratory for Turbulence Research in Aerospace and Combustion, Department of Aerospace and Mechanical Engineering, Monash University, Clayton, Victoria, 3800, AUSTRALIA

Department of Aeronautical Engineering, King Abdulaziz University, Jeddah, Kingdom of Saudi Arabia

* Corresponding author: m.khashehchi@uq.edu.au

Abstract Tomographic Particle Image Velocimetry (TPIV) was used to study the initial transition process formed in a free jet between the laminar flow at the jet exit, and the fully turbulent flow region at Re=6500. The evolution of the turbulence characteristics in this particular region has been assessed by means of the invariants of the Velocity Gradient Tensor (VGT). These invariants enable us to study the dynamics, geometry and topology of the flow. A mapping from the three-dimensional flow fields to a two dimensional invariants plane is used to analyze the dissipation of kinetic energy at small scales and the amplification of local vorticity due to vortex stretching. A systematic study of the event that represents the persistent alignment of the vorticity vector with the second eigenvector of the rate of strain tensor was examined, and the results of this phenomenon at the near-field of the jet are discussed. Results show that vorticity vector, ω, maintains its alignment with the intermediate eigenvector of the rate of strain tensor, υ_2, in the developing region by either the rotation of the intermediate eigenframe or the tilting of ω.

1. Introduction

Understanding the evolution and subsequent dynamics of small-scale motions (e.g. vorticity and rate-of-strain fields) in the three-dimensional turbulent round jet is of primary importance, not only for the motions contributing to the generation of turbulence and their usefulness in evaluating different physical models, but also because they comprise a reference for related engineering applications. Although most of the past studies have been focused on the statistical description of the self-similar fully turbulent region of jets, a considerable attempt, starting with the works of Brown and Roshko [1974b], was made to understand the developmental behavior of free shear layers and free turbulent jets. It is well known that, for instance, the initial instability of the laminar shear layer near the nozzle is followed by a convected periodic vorticity shape and consequently formation of a periodic street of vortex rings (Yule [1978]). These structures continuously grow as

they move downstream before breaking down into complex structures. The role of three-dimensional large-scale structures in the evolution of the above mechanism has been marked in several works (see e.g. Martin and Meiburg [1991], Ganapathisubramani et al. [2002] and Liepman and Gharib [1992]). In most cases, the studies have focused on the areas near both vortex cores and the regions between successive vortex cores in the shear layer called “braids”. For example, the experiments of Liepman and Gharib [1992] who examined planes normal to the axis of a water jet with a Reynolds number of 5500, indicates that three-dimensionality first developed in the braid regions.

Unlike the large-scale (vortical) structures, which are mainly characterized by the velocity field itself, the small scales are always associated with the field of velocity gradients. These gradients play an essential role in the dynamics of the small-scale characteristics such as vorticity and strain fields. The evolution of the velocity gradients is of primary importance because they govern the mechanism of vortex-stretching. Unlike temporal evolution, studies of spatial evolution are lacking in the literature because up to now they have been very difficult to be obtained by experimental methods. The main objective of the presented study is a systematic analysis of the small scale dynamics in the near-field region of a turbulent round jet. The emphasis is on processes involving the fields of invariants of the velocity gradient, rate of strain and rate of rotation tensors as well as enstrophy and strain product terms that appear in their transport equations.

Here, special emphasis is on the variation of the universal features of the invariants; e.g. the general “tear-drop” shape of the *R*-*Q* map (see e.g., Ooi *et al*. [1999]), with the distance to the nozzle. The experimental arrangement, measurements and analysis of the acquired data are described in section 2. The analysis of the invariants of the velocity gradient, rate of strain and rate of rotation tensors through the developing near-field area, is described in section 3. Section 4 describes the evolution of the small scale properties of the flow in the near field region of the round jet. Concluding remarks are in section 5.

2. Experimental setup

The basic aim of this experiment was to study the near-field region of the axisymmetric round jet. The jet, shown in figure 1, consisted of a concentric aluminium tube (76.2mm in diameter) with an entrance for pressurized air on one side and an exit nozzle following a cubic curve-fit with a 25mm diameter outlet on the other side, which yields a contraction ratio of 9:1 that terminates in a 25mm straight cylindrical section. A sharp-edge of the jet was achieved by machining the leading area of the jet. The jet was driven by a centrifugal blower yielding a maximum outlet velocity of 50 m/s. The air is supplied to the jet by the blower along the inner tube via a thin rubber coupling which isolates the nozzle from vibration. The turbulence level at the exit was found to be less than 0.8 % at the highest exit velocity. Exit velocity of the nozzle was obtained via a Pitot-tube.

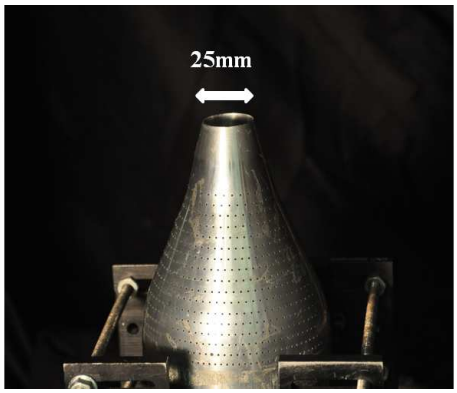

Fig. 1 Jet apparatus with diameter of 25mm

The basic optical and electronic equipment, as well as the methodology, are the same as one described in the earlier publication by Khashehchi *et al*. [2010]. However, here the size of the jet is more than 12 times bigger than the size of the jet used by Khashehchi *et al*. [2010], and four smaller lenses (105mm Sigma lenses) were used which provided a magnification of 0.36. Furthermore, since two of the cameras record backward scattered light (low intensity), a mirror was placed in front of the laser sheet after the jet to reflect back the laser light to the plane of the laser sheet. This can create a uniform light intensity for forward- and backward-scattered laser light. The observation volume of approximately 100 × 75 × 4 mm^3 was chosen with respect to the recording magnification. The characteristic properties of the flow are: exit velocity 4 m/s and Re_d = 6500 (based on the nozzle diameter).

The three components-three dimensional velocity field of the jet was measured using tomographic PIV (Elsinga et al [2006], Atkinson & Soria [2009]). In order to improve the quality of reconstructed voxel intensities, three image pre-processing algorithms were applied to all images: background intensity removal, local intensity rescaling and Gaussian smoothing (3 × 3 kernel size). The volume was divided into small voxel cubes with the resolution 100 voxels/mm and the voxel intensity was reconstructed using the MART algorithm with 5 iterations. For the 4mm thick light sheet, dimensions of the reconstructed volume are 100×75×4mm corresponding to 4008×2672×400 voxels. The volume frame pairs were interrogated with 44×44×44 interrogation volume size with 75% overlap. The displacement vector within each interrogation volume was obtained using a 3D FFT-based cross-correlation algorithm with iterative multigrid and window deformation (Scarano and Riethmuller [2000]). Each volume yielded 224 × 148 × 13 (430976) velocity vectors with a spatial resolution of 0.44mm. Figure 2 shows an example of the instantaneous velocity field obtained by TPIV. Data validation based on a signal-to-noise ratio threshold of 1.2 and on the normalized median test with a maximum threshold of 2 (Westerweel and Scarano [2005]) returned 5% spurious vectors. The average signal-to-noise ratio and normalized correlation coefficient were 3.3 and 0.6, respectively, for a particle image density of 0.08 ppp (particle per pixel).

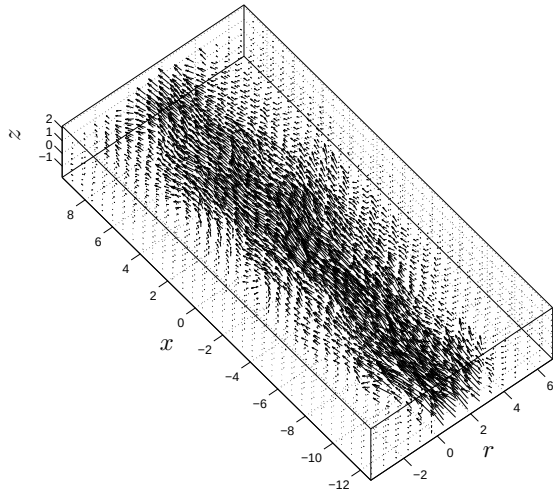

Fig. 2 Example of the instantaneous velocity field obtained by the TPIV

Results of the TPIV experiment were assessed through an analysis of some of the single point statistics such as the mean axial velocity and the Reynolds shear stress. They will be used to study the evolution of the turbulence characteristics along the centreline of the jet. For the mentioned flow configuration, the statistics were obtained through an ensemble average over the number of records acquired. Note that, since the aim of this experiment was to study the near field region, the profiles do not show a self-similarity pattern and only the evolution of the profiles will be presented.

Figure 3 shows the mean axial velocity and Reynolds shear stress profiles for several near-field locations. The profiles are symmetric within the PIV spatial resolution and show the evolution of the mentioned statistics for *x/d* = 0 to 6. Under the "top−hat" velocity profile at the jet exit assumption, the mean centreline velocity *U* is constant along the potential core. The mean axial velocity profiles normalized with the mean centreline velocity (U_c) for the TPIV results are shown in figure 3-a. Figure 3-b shows the Reynolds shear stress normalized by the square of the centreline velocity U_c^2. The maximum Reynolds stress is moved toward the jet centreline with increasing downstream distance. Since the jet is expanding in all directions, the component *v* has negative and positive values at both sides of the jet. Therefore, the Reynolds shear stress distribution, *uv*, must be positive for *r>0*.

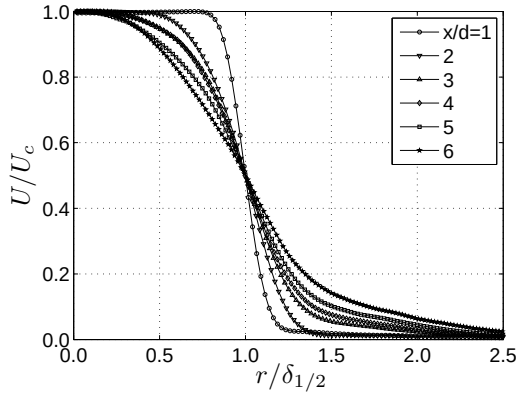

(a)

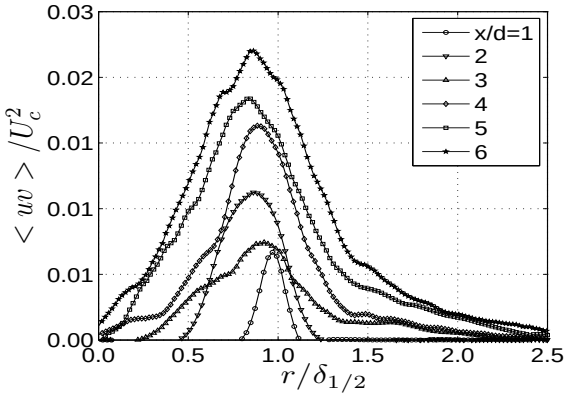

(b)

Fig. 3 Profiles of several first and second order statistics of the jet centreline at different axial positions. a): mean axial centreline velocity and b): Reynolds shear stress

.

3. Evolution of the Invariants of the Velocity Gradient, Rate of Strain and Rate of Rotation Tensors

3.1. Analysis of the Invariants *R* and *Q* along the Centerline Axis

The second and third invariants of the VGT (*R* and *Q*), are analyzed along the centerline axis from the jet exit, in order to analyze the relationship between the flow topology and dynamics. Results of 300 volume samples in the near-field region (x/d < 6) of the jet including 129,292,800 (148 × 224 × 13 × 300) data points will be presented in this section. The scatter of the second and third invariants of VGT, *R* and *Q*, in the near field region of the jet (at the jet exit) is plotted in figure 4-a. As can be seen from the graph, most of the data points are accumulated around the origin. As introduced by Chong et al. [1990], each quadrant of the *R*-*Q* map has a physical description. Unlike the fully turbulent region, where the points have a strong tendency toward the lower-right region of the *R*-*Q* map (defined as Unstable-Node/Saddle/Saddle, UN/S/S) and toward the second quadrant of the *R*-*Q* plane (defined as Stable-focus/Stretching, SF/S), there is no concentration of the data points in any particular region of the map. As a consequence, the general shape of the scattered data points appears as a nominally elliptical.

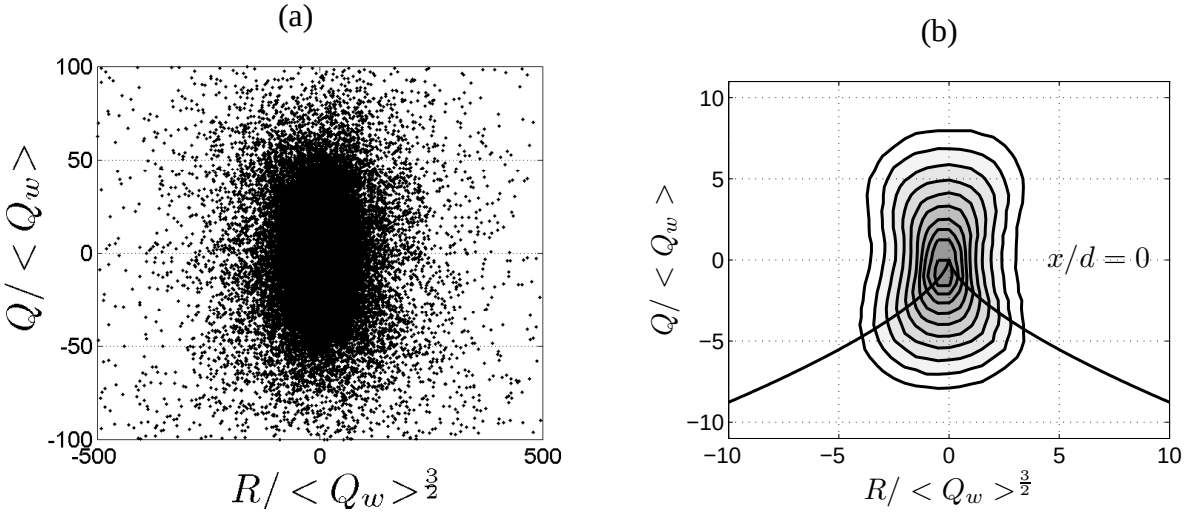

Fig. 4 Scattered (a) and contour (b) plots of jpdf of the invariants of the VGT at x/d = 0

To better understand the physics of the flow, especially for the data points near the origin, it could be useful to look at the joint pdf (jpdf) of data points in *R*-*Q* map (figure 4-b). As mentioned above, the general shape of the jpdf at the laminar region, the characteristic “tear-drop” shape of the *R*-*Q* phase-map, is not appeared yet. The values of *R* and *Q* exist only in the vertical ellipse around the origin with no concentration in the region of positive or negative *R*. This agrees with what has been noted by Blackburn *et al*. [1996]: that in the laminar region in an ideal flow (e.g. laminar near field region), there is only one dominant component of the velocity (U component). This velocity produces two components of the velocity gradient in the two other directions (dU/dy and dU/dz) and the velocity gradient tensor takes the degenerate form;

$$A \approx \begin{pmatrix} 0 & \partial U/\partial y & \partial U/\partial z \\ 0 & 0 & 0 \\ 0 & 0 & 0 \end{pmatrix}$$

This tensor produces zero *R* and *Q*, but *R* tends to be zero in the order of $|A|^3$ (where |A| is the determinant of the matrix A) while this tendency for the *Q* is $|A|^2$. Therefore, with a small divergence error in the experimental results where the continuity equation is not satisfied, the data points are scattered around their origin as a vertical ellipse. Moreover, a nonzero level of turbulence in that area causes nonzero values of *R* and *Q*.

The mean profiles of the invariants along the jet centerline in relation to the distance from the jet exit are shown in figure 5. To enable a clear understanding of the graphs, a polynomial curve is fitted to both graphs and is shown with the symbols. The evolution of the invariants *R* and *Q* shows that in the jet exit (x/d=0) both invariants are zero, which is expected. Furthermore, it is obvious that the rate of change of *Q* is much greater than for R. Surprisingly, the mean value of *R* continues at about zero value until x/d=3, fluctuating around zero till x/d=6. Note that deep inside the turbulent region (x/d > 10), mean values of *R* and *Q* are zero.

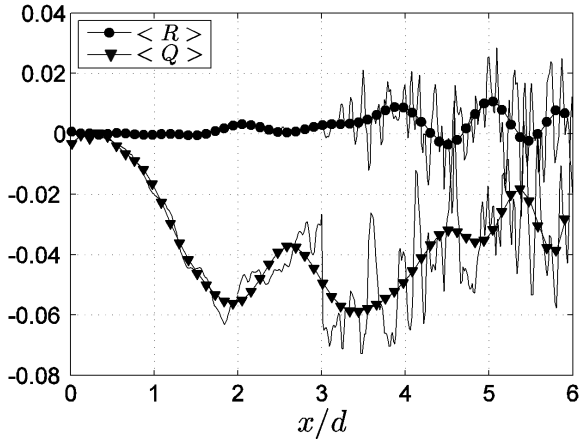

Fig. 5 Mean spatial evolution of the invariants of the VGT along the centerline axis of the jet where symbols indicate a polynomial curve-fit.

The influence of the different distances from the jet exit on the values of the invariants can be seen in the jpdf contours shown in figure 6 (a-f). In all plots, the values of *R*, *Q* are normalized with the mean Q_w (second invariant of rate of rotation tensor). As seen from the graphs, the general "tear-drop" shape of the jpdf is formed after x/d=2, evolving toward a self-similar pattern at around x/d=3, and remaining self-similar afterward downstream of the flow.

It is seen that after x/d=3 all the graphs show an approximate self-similar "tear-drop" shape, indicating that most data points in the flow have local topology SF/S and UN/S/S. The tendency for data points to "hug" the D=0 line (discriminant line) when the local topology of the flow is UN/S/S is similar to that seen in the mixing layer by Soria *et al*. [1996], as well as in the channel flow studied by Blackburn *et al*. [1996].

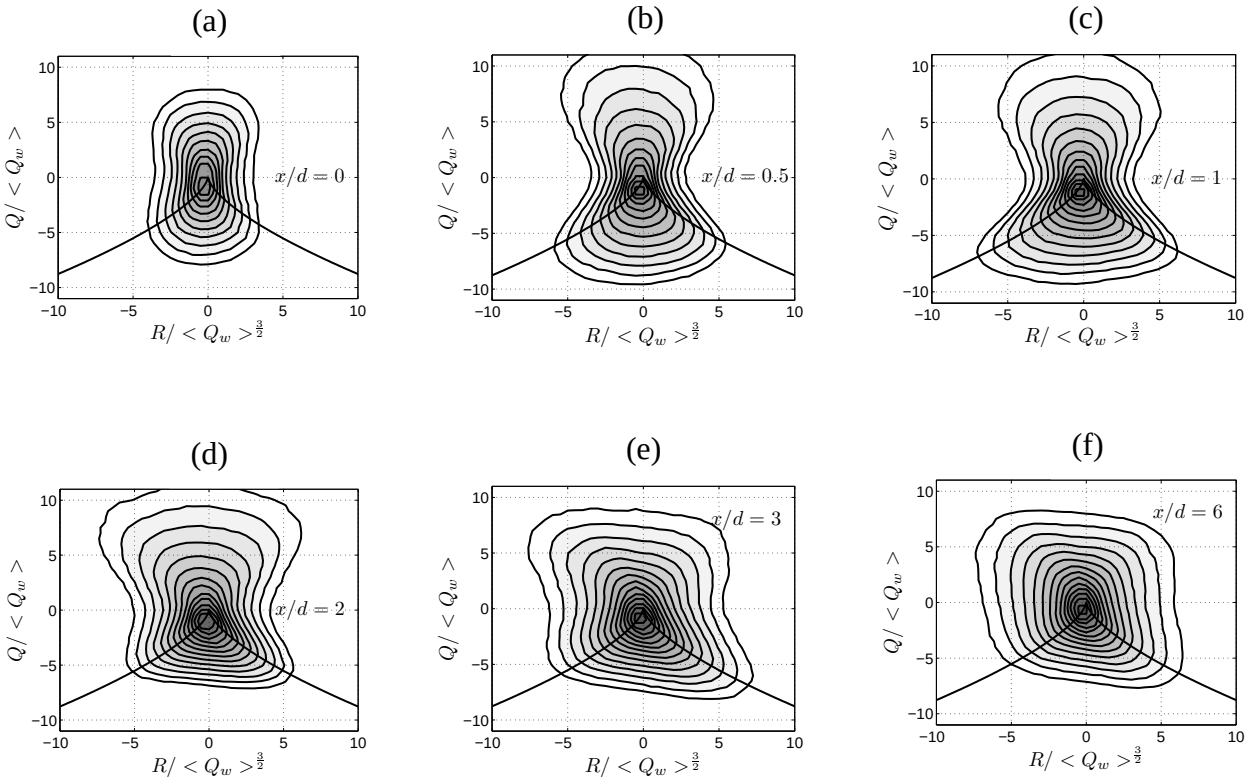

Fig. 6 Evolution of the jpdf of the invariants of the VGT for x/d = 0 to 6.

3.2. Analysis of the Invariants R_s and Q_s along the Centerline Axis

The tensor S_{ij} is the symmetric part of VGT and its invariants can be measured in the same way as they were computed for VGT. The rate of strain is a trace-free, symmetric tensor which yields three real eigenvalues, and in the R_s-Q_s map all data points scatter in the region below the discriminant line ($D_s=27R_s^2+4Q_s^3$), and any deviation from this region could be taken into account as experimental error exists in the measurements. Figure 7 shows the jpdf of the second and third invariants of the rate of strain tensor (R_s and Q_s), as a function of distance from the jet exit. Again, the invariants are normalized with the mean Q_w and the contour levels presented are the same as those used in the R-Q plot. In the fully turbulent jet, we expect to see the data on the lower right quadrant, but as can be seen from figure 7-a, this tendency is not observed at x/d=0. In this region, there are data points with high kinetic energy dissipation without any effect of enstrophy density. If we assume $\lambda_3 > \lambda_2 > \lambda_1$, eigenvalues of the rate of strain tensor, the ratio of the eigenvalues for this particular region is 1:0: -1, which means the rate of strain is essentially two dimensional.

Further away from the jet, there is a marked tendency for the data points to be skewed toward the right hand side (fourth quadrant) of the lower area of the R_s-Q_s map. This pattern is in reasonable agreement with the works of Blackburn *et al*. [1996], Soria *et al*. [1996] and Da-Silva and Pereira [2008]. In this area (x/d > 3), the rate of strain tensor has two positive and one negative eigenvalue. Again, the contours appear to show a self-similar pattern just after x/d=3.

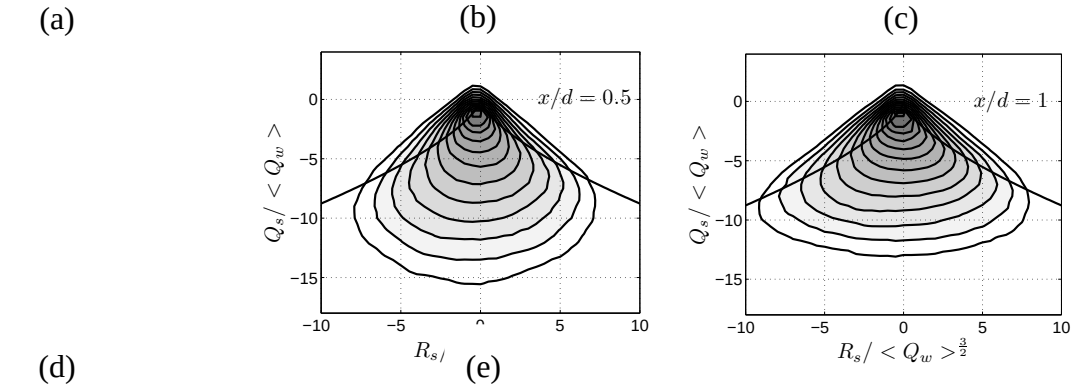

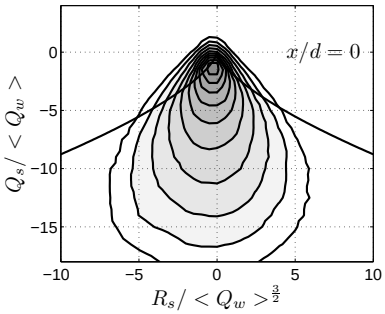

Fig. 7 Evolution of the jpdf of the invariants of the rate of strain tensor for x/d = 0 to 6.

It is seen that in the near field of the jet (x/d<3), the contour shows a symmetric pattern around the line Q_s=0. This is due to the tendency of the R_s to be zero as $|S|^3$ while Q_s is negative. These quantities of R_s and Q_s create a vertical ellipse shape below the discriminant line D_s=0 (f)

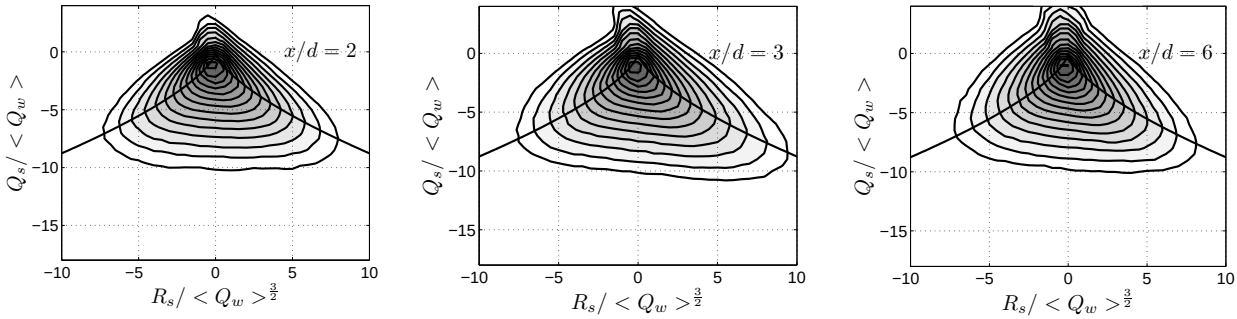

and the eigenvalues show the ratio of 1:0:-1. As the flow evolves and turbulence intensifies, the contours show that the rate of strain is definitely three dimensional and the tendency for the data to fall in the lower right quadrant with a few excursions to the left side of the Q_s axis becomes more pronounced (x/d>3). Eigenvalues of the rate of strain tensor in this region have the ratio of 2.5:1:-3.4. Note that the most probable eigenvalue ratios observed in several works are 3:1:-4 and 2:1:-3 (Ooi *et al*. [1999], Soria *et al*. [1996] and Blackburn *et al*. [1996]).

3.3. Analysis of the Invariants Q_w and $-Q_s$ along the Centerline Axis

The study of the second invariants of the rate of strain and rate of rotation tensors will be investigated in order to analyze the geometry of the dissipation and enstrophy fields. Figure 8 shows the jpdf between the second invariant of the rate of rotation and rate of strain tensors, Q_w and $-Q_s$, respectively, as a function of distance from the jet exit. Data that lies on the horizontal axis (i.e. along Q_w) represents points in the flow where there is high enstrophy with small dissipation and data points that scatter around the $-Q_s$ axis represent regions with a high level of dissipation without any rotation. In a flow with one dominant velocity component (flow at the jet exit), the velocity gradient tensor has just two non-zero components ($\partial U/\partial y$ and $\partial U/\partial z$). Consequently, rate of strain and rate of rotation tensors have four non-zero components:

$$S \approx \frac{1}{2}\begin{pmatrix} 0 & \partial U/\partial y & \partial U/\partial z \\ \partial U/\partial y & 0 & 0 \\ \partial U/\partial z & 0 & 0 \end{pmatrix}$$

and

$$W \approx \frac{1}{2}\begin{pmatrix} 0 & \partial U/\partial y & \partial U/\partial z \\ -\partial U/\partial y & 0 & 0 \\ -\partial U/\partial z & 0 & 0 \end{pmatrix}$$

The second invariant of these two tensors is

$$Q_s = -\frac{(\partial U/\partial y)^2 + (\partial U/\partial z)^2}{4} \qquad (1$$

$$Q_w = \frac{(-\partial U/\partial y)^2 + (-\partial U/\partial z)^2}{4} \qquad (2$$

Equations 1 and 2 indicate that in the laminar region $Q_w = -Q_s$. On the other hand, figure 8-a shows that early in the evolution of this flow, most data points tend to be aligned in the 45° line which means a high correlation between dissipation and enstrophy. This flow is associated with two dimensional vortex sheet structures. As the flow evolves, this correlation between $-Q_s$ and Q_w collapse into a wider region and further away from the jet the distributions have a completely different character; all data is distributed in the $-Q_s$ and Q_w map with a slide tendency toward Q_w axis. In this region (x/d=3), the patterns resemble the work of Blackburn *et al.* [1996] and Ooi *et al.* [1999].

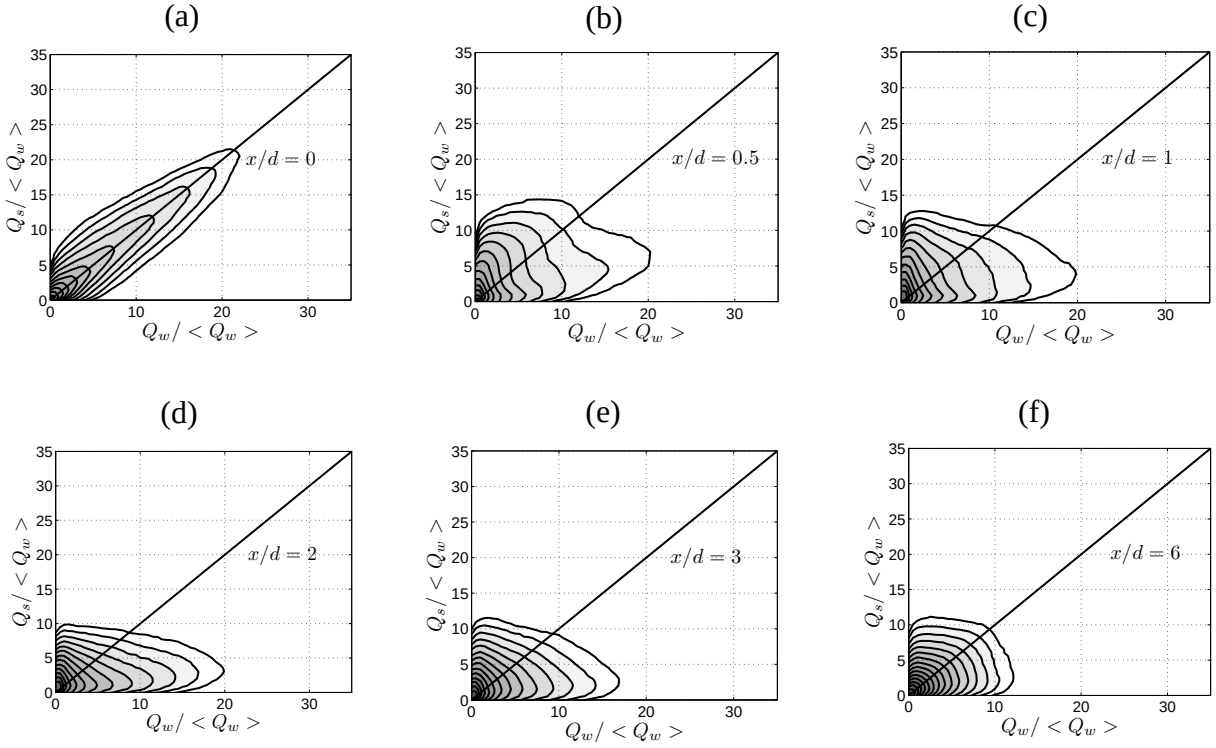

Fig. 8 Evolution of the jpdf of the $-Q_s$ *and* Q_w for *x/d* = 0 to 6.

Notice that at x/d>3, for the contour lines associated with the most frequent values, there is still some tendency for the lines to be aligned with the inclined 45° line. Indeed, as in Ooi *et al.* [1999] the contour lines of intense values of Q_w are slightly skewed toward the axis $-Q_s = 0$, which suggests that intense values of Q_w correspond to much smaller values of $-Q_s = 0$, i.e., the high Q_w regions are associated with solid body rotation with little energy dissipation.

4 Vorticity Alignment

This section focuses on the statistical analysis of the jet flow information during its evolution in the near field region of the round jet. The purpose of studying the evolution of the properties along the centerline is to evaluate the systematic study of the event that represents the persistent alignment of the vorticity vector with the second eigenvectors of the rate of strain tensor (Tsinober [2001]). The evolution of the several quantities (production and destruction terms of the vorticity and strain transport equations as well as enstrophy and strain product terms) along the centerline of the jet starting from the nozzle are plotted in figure 9-left. As is clear, the enstrophy production term $\omega_i\omega_j S_{ij}$ is small and positive. Perhaps, the nature of the eigenvalues of the rate of strain tensor ($\lambda_1 < 0$ and $\lambda_3 > 0$) is the reason for the $\omega_i\omega_j S_{ij}$ to remain small at all regions. Put simply, the enstrophy production term can be represented in its term associated with the eigenvalues (λ_i) and eigenvectors (υ_i) of the rate of strain tensor (i=1, 2, 3, indicates the axial, radial and azimuthal directions, respectively),

$$\omega_i\omega_j S_{ij} = \omega^2(\lambda_1 cos^2(\upsilon_1,\omega) + \lambda_2 cos^2(\upsilon_2,\omega) + \lambda_3 cos^2(\upsilon_3,\omega)). \quad (3$$

The substantial alignment between ω and λ_2 for the entire region x/d = 0 to 6 causes $\cos(\upsilon_2,\omega)$ to be approximately equal to 1. This value multiplied by low values of λ_2 makes term $\lambda_2\cos^2(\upsilon_2,\omega)\sim 0$. In addition, the large positive value of λ_3 is also canceled by a large negative λ_1 to keep the total $\omega_i\omega_j S_{ij}$ small (figure 9-right).

The interaction between ω and S_{ij} , one of the most important dynamical aspects of 3D-turbulence, depends on the magnitude of ω and S_{ij} as well as on the geometry of the field of velocity derivatives. An example of the special dynamical importance is the strict alignment between ω and υ_2, the second eigenvector of the rate of strain tensor. Figure 10 shows the spatial evolution of the angle between ω and the eigenvectors, υ_i, of the rate of strain tensor along the centerline axis x/d=0 to 6. To make a convenient representation of the alignments, since $\cos^2(\upsilon_1,\omega)+\cos^2(\upsilon_2,\omega)+\cos^2(\upsilon_3,\omega) = 1$, $\cos^2$ of the angles between ω and υ_i is shown. From figure 10, we observe that the mentioned alignment between ω and υ_2 (in comparison to the two other directions) is significant throughout most regions from the jet exit. On the other hand, except for the first couple of x/d where this alignment drops and ω loses its alignment with the intermediate eigenvector, the vectors ω and υ_2 maintain and improve their alignment for the rest of the developing area. A comparison between the solid symbols for x/d=1 and 6 in the figure 10 indicates that in the far-field region (x/d=6) vorticity is more highly aligned with υ_2 than in the near field region. Contrary to the persistent alignment of vorticity to υ_2, the alignment between ω and two other eigenvectors, υ_1 and υ_3, shows different patterns. Initially, near to the jet exit, ω has the same angle with both υ_1 and υ_3 (figure 10), whereas away from the jet (x/d>3), the alignment between ω and υ_3 falls down and these two vectors are nearly perpendicular to each other.

The mechanism of ω-υ_2 alignment after x/d=1 can be analyzed by looking at the evolution of the vorticity and eigenvectors of the rate of strain tensor, υ_i, along the centerline axis. It seems that both ω and υ_i are participating in this evolution, as shown in figure 11, where the spatial evolution of the absolute orientations of ω and υ_i along the jet centerline are presented. This figure shows the rotation of both ω and υ_i in the near-field developing area with respect to a rigid coordinates (e_1, e_2, e_3). During this evolution three significant events happen.

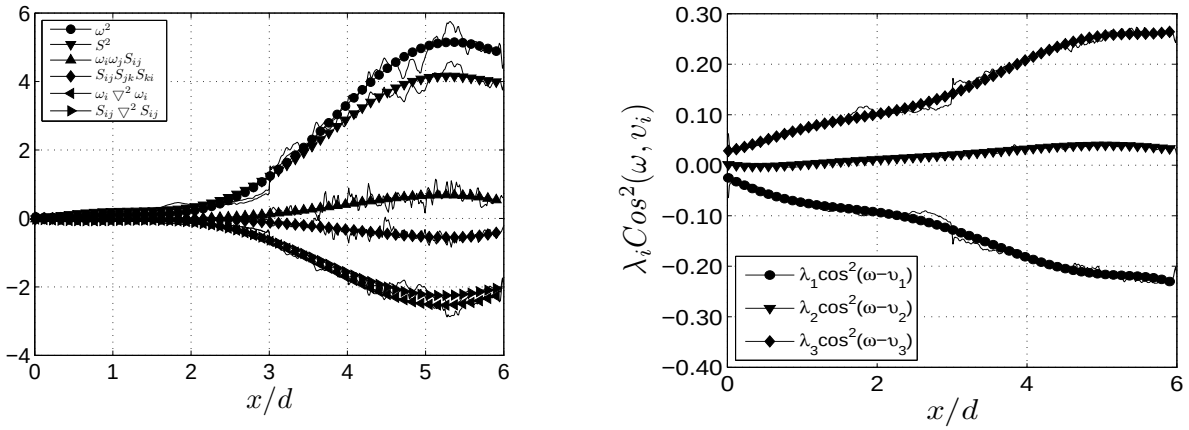

Fig 9 Evolution of the parameters: Left) ω^2, S^2, $\omega_i\omega_j S_{ij}$, $-S_{ij}S_{jk}S_{ki}$, $\nu\omega_i \bigtriangledown^2 \omega_i$ and $\nu S_{ij} \bigtriangledown^2 S_{ij}$, Right) $\lambda_i \cos^2(\omega, \upsilon_i)$, along the jet centerline for x/d = 0 to 6.

First, just after the jet exit at x/d = 0, all eigenvectors start to rotate with respect to the coordinates e_1, e_2, e_3, reaching a more or less stable orientation up to x/d=3 (figure 11 b to d). At a certain regions, υ_1 and υ_3 are oscillating in the plane e_1-e_2, while their angle with e_3 remains larger than the others. Secondly, for the entire region, ω rotates slightly around the rigid coordinates and at x/d=5, ω is located such that its angles relative to all three directions are identical. Namely, the end

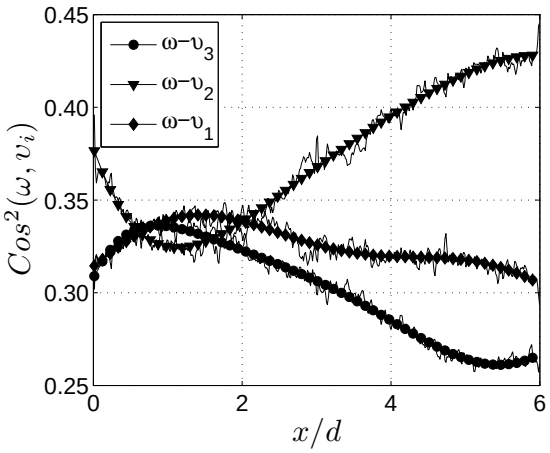

Fig. 10 Mean spatial evolution of the angle between ω, υ_i along the centerline axis.

of the potential core where both shear layers approach together and the transient region starts. Finally, at the near-field region (x/d < 2), where the second eigenvector rotates toward the third coordinates and when both υ_1 and υ_3 fluctuate in the plane e_1-e_2, it is seen how ω also starts to rotate (tilt) and change its direction toward the third coordinate e_3, but at a slower rate. Subsequently, the alignment between ω-υ_2 is reinstated and the value of $\cos^2(\omega,\upsilon_2)$ starts to increase, and both $\cos^2(\omega,\upsilon_1)$ and $\cos^2(\omega,\upsilon_3)$ decrease with different slopes. In summary, two mechanisms are responsible for the mutual activities of ω and υ_i, namely the rotation of the eigenvectors, υ_i, and the tilting of ω.

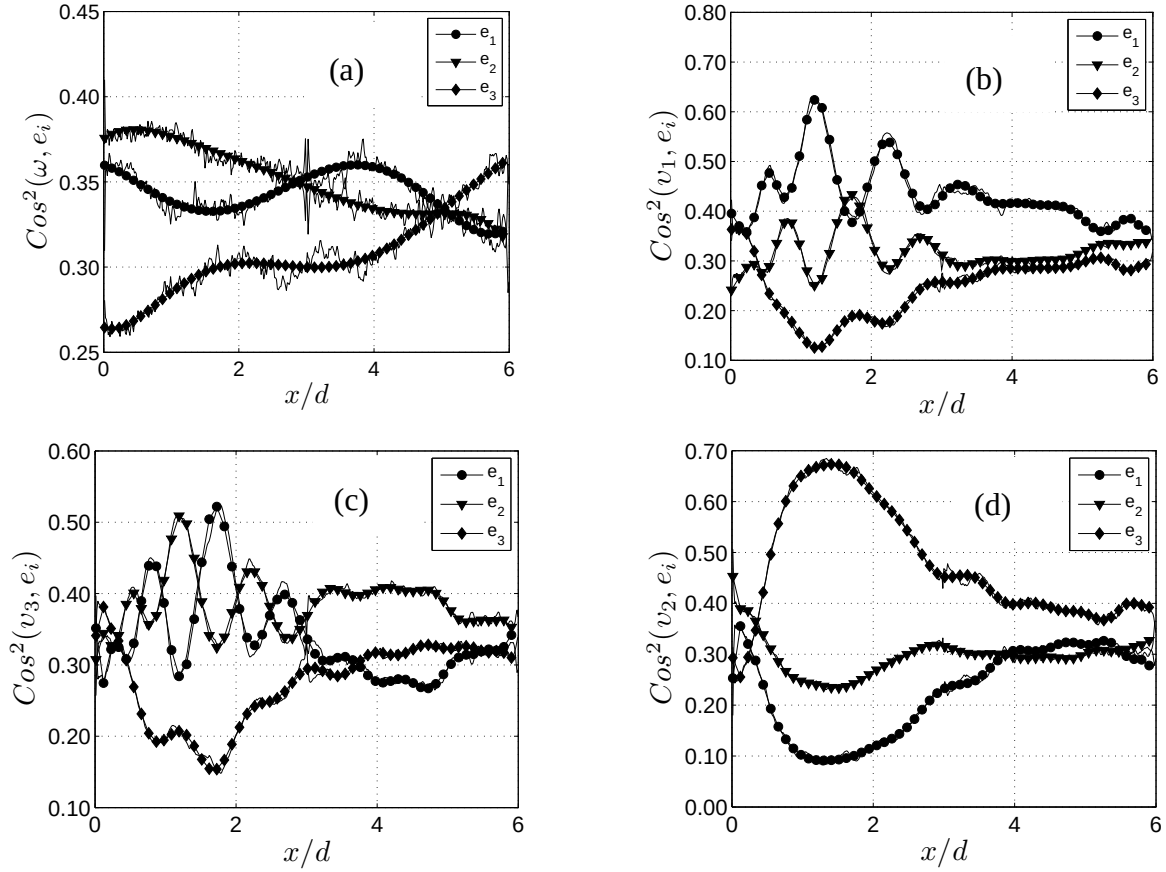

Fig 11 Evolution of the orientation of the υ_i and ω with respect to a fixed reference system e_i for x/d = 0 to 6.

5. Conclusions

TPIV results were performed in the developing near-field area of the turbulent round jet. The analogy of the invariants of the velocity gradient, rate of strain and rate of rotation tensors was applied in this particular region to analyze the evolution of the flow characteristics along the jet centerline from the laminar to the turbulent state. The instantaneous value of the invariants of the VGT is zero in the jet exit. These values evolve toward the fully turbulent region, showing the universal "tear-drop" pattern of turbulence, at around x/d=3. The same pattern is repeated for the other invariant maps R_s-Q_s and Q_s-Q_w.

Small scale enstrophy and strain dynamics are also analyzed in the developing near-field area of the jet. Results show that ω is aligned with υ_2, the eigenvector corresponding to the intermediate eigenvalue of the rate of strain tensor, at the jet exit and that it maintains this alignment in the developing region by two different mechanisms; namely, the rotation of the intermediate eigenvector and the tilting of ω.

6 References

Atkinson C, Soria J (2009) An efficient simultaneous reconstruction technique for tomographic particle image velocimetry. *Exp in Fluids*, 47: 553–568.

Blackburn H M, Mansour N N, Cantwell B J (1996) Topology of fine-scale motions in turbulent channel flow. *J Fluid Mech.*, 310:269–292.

Brown G.L, Roshko A (1974b) On density effects and large structure in turbulent mixing layers. *J Fluid Mech*, 64:775–816.

Chong M S, Perry A E, Cantwell B J (1990) A general classification of three-dimensional flow fields. *Phys of Fluids A*, 2:765–777.

Da-Silva B C, Pereira J C F (2008) Invariants of the velocity-gradient, rate-of-strain, and rate-of-rotation tensors across the turbulent/ non-turbulent interface in jets. *Phys of Fluids*, 20, 055101.

Elsinga G E, Scarano F, Wieneke B, van Oudheusden B W (2006) Tomographic particle image velocimetry. *Exp in Fluids*, *41*: 933–947.

Ganapathisubramani B, Longmire E K, Marusic I (2002) Investigation of three dimensionality in the near field of a round jet using stereo PIV. *Journal of Turbulence*, 3:1–12.

Khashehchi M, Elsinga G E, Ooi A, Soria J, Marusic I (2010) Studying invariants of the velocity gradient tensor of a round turbulent jet across the turbulent/nonturbulent interface using TPIV. 15th Int Symp on Applications of Laser Techniques to Fluid Mechanics, Lisbon, Portugal.

Liepman D, Gharib M (1992) The role of streamwise vorticity in the near-field entrainment of round jets. *J Fluid Mech*, 245:643–668.

Martin J E, Meiburg E (1991) Numerical investigation of three-dimensionally evolving jet subject to axisymmetric and azimuthal perturbations. *J Fluid Mech*, 230:271–318.

Ooi A, Martin J, Soria J, Chong M S (1999) A study of the evolution and characteristics of the invariants of the velocity-gradient tensor in isotropic turbulence. *J Fluid Mech.*, 381:141.

Scarano F, Riethmuller M L (2000) Advances in iterative multigrid PIV image processing. *Exp in Fluids*, *Suppl*:*S*51–*S*60.

Soria J (1996) An investigation of the near wake of a circular cylinder using a video-based digital cross-correlation particle image velocimetry technique. *Experimental Thermal and Fluid Science*, 12:221-233.

Tsinober A. *An informal introduction to turbulence.* Springer, Berlin and New York, ISBN 978-1-4020-0166-6, 2001.

Westerweel J, and Scarano F (2005) A universal detection criterion for the median test. *Exp in Fluids.*, 39:1096–1100.

Yule A J (1978) Large-scale structure in the mixing layer of a round jet. *J Fluid Mech*, 89:413–432.